4ICEGE
Thessaloniki-GREECE 2007

4th International Conference on
Earthquake Geotechnical Engineering
June 25-28, 2007
Paper No. 1458

A CONTACT INTERFACE MODEL FOR NONLINEAR CYCLIC MOMENT-ROTATION BEHAVIOR OF SHALLOW FOUNDATIONS

Sivapalan GAJAN [1] and Bruce KUTTER[2]

ABSTRACT

It has been recognized that the ductility demands on super structure might be reduced by allowing rocking behavior and mobilization of the ultimate capacity of shallow foundation, particularly for shear wall structures. However, the absence of practical reliable foundation modeling techniques and the uncertainty in soil properties have hindered the use of nonlinear soil-foundation-structure interaction as a designed mechanism for improving performance of a soil-foundation-building system. This paper presents a new "contact interface model" that has been developed to provide nonlinear constitutive relations between cyclic loads and displacements of the footing-soil system during combined loading. The rigid footing and the soil beneath the footing in the zone of influence, considered as a macro-element, were modeled by keeping track of the geometry of the soil surface beneath the footing along with the kinematics of the footing-soil system. The coupling between forces is incorporated in the model through tracking the geometry of the contact interface, interaction diagrams, and the critical contact length ratio; the ratio of the minimum length of the footing required to support the vertical and horizontal loads. Several contact interface model simulations were carried out and the model predictions are compared with centrifuge experimental results that have a wide range of initial static vertical factor of safety. It is shown that the footing-soil contact interface model captures the essential features of the cyclic load-deformation behavior that were observed in the centrifuge experiments. The contact interface model predictions for moment capacity, rotational stiffness, energy dissipation, and permanent deformations compare reasonably well with the centrifuge experimental results.

Keywords: Shallow foundation, rocking, macro-element model, soil-foundation interaction

INTRODUCTION

Soil-foundation interaction associated with heavily loaded shear wall structures during large seismic events may produce highly nonlinear load-displacement behavior. Geotechnical components of the foundation are known to have a significant effect on the building response to seismic shaking (Taylor et al., 1981, Faccioli et al., 2001, and Gajan et al., 2005). The nonlinearity of the soil may provide energy dissipation and serve as a fuse mechanism, potentially reducing shaking demands exerted on the structural components of the building, particularly for shear wall structures. Performance based earthquake engineering design methods emphasize the importance of incorporating the nonlinear soil-foundation-structure interaction in design. In order for structural and geotechnical engineers to make use of the advantages of nonlinear soil-foundation-structure interaction and to use optimum energy dissipation mechanisms in structural elements and foundation soil, reliable structural and foundation constitutive models are necessary. Since the rocking of shallow foundation and soil yielding may

[1] Assistant Professor, Department of Civil Engineering, North Dakota State University, Fargo, ND, USA. Email: s.gajan@ndsu.edu
[2] Professor, Department of Civil & Environmental Engineering, University of California, Davis, CA, USA. Email: blkutter@ucdavis.edu

result in permanent deformations at foundation level, it is important to have soil-foundation interface models that are capable of predicting the load capacities, stiffness degradation, energy dissipation and the resulting permanent and cyclic deformations at the foundation.

This paper introduces a new "contact interface model" that provides nonlinear constitutive relations between cyclic loads and displacements at the footing-soil interface of a shallow foundation that is subjected to combined loading. The rigid footing and the soil beneath the footing in the zone of influence, considered as a single macro-element, were modeled by keeping track of the geometry of the soil surface beneath the footing, along with the kinematics of the footing-soil system, and with the introduction of a new parameter, critical contact length ratio, Lc/L; where L is the length of the footing in the direction of loading and Lc is the minimum length of the footing required to have contact with soil to support the vertical and shear loads. The contact interface model allows the coupling between forces and displacements when the foundation is subjected to combined loading that causes soil yielding and footing uplift simultaneously. The comparisons of contact interface model simulations with centrifuge experimental results for shear wall structures supported by shallow foundations are also presented in the paper.

Other researchers have used macro-element concepts to model the load-displacement behavior of structural elements and shallow foundations (Nova and Montrasio, 1991, Cremer et al., 2001, Houlsby and Cassidy, 2002). Most of the previous attempts with macro-element models for shallow foundations describe the constitutive relations based on yield surfaces, potential surfaces, and flow rules in generalized load space. The macro-element contact interface model presented in this paper differs in the sense that the constitutive relations are obtained by tracking the evolution of maximum shape of the gaps and the geometry of the contact interface.

CONTACT INTERFACE MODEL

Fig. 1 illustrates the concept of macro-element modeling and the forces (vertical, V, shear, H, and moment, M) and displacements (settlement, s, sliding, u, and rotation, θ) at the footing soil interface when the foundation is subjected to combined loading. The macro-element contact interface model includes the constitutive relations that correlate the forces (V, H and M) and displacements (s, u, and θ) at the footing-soil interface during combined cyclic loading. In numerical modeling point of view, the contact interface model is placed at the footing-soil interface, replacing the rigid foundation and surrounding soil in the zone of influence.

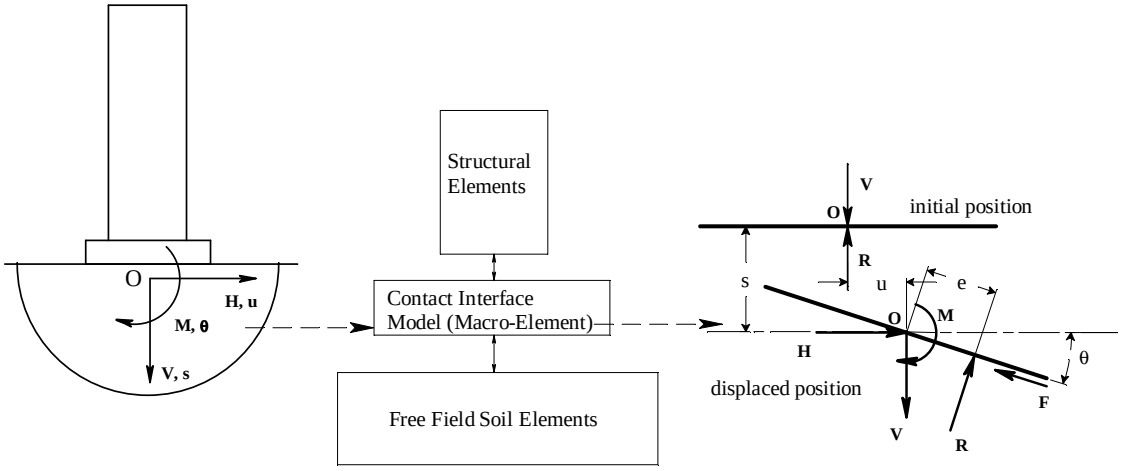

Figure 1. Forces and displacements at footing-soil interface and the concept of macro-element modeling of shallow foundation

When incremental displacements are given to the macro-element model as input, it returns the corresponding incremental loads and vise versa. This paper describes how the moment-vertical load, moment-rotation, and settlement-rotation behavior were modeled in contact interface model and how the coupling between vertical force, bearing pressure distribution and moment is handled. The relationship between horizontal force-sliding, settlement-sliding and the coupling between horizontal force, vertical force and moment are out of scope of this paper (for more details, see Gajan, 2006).

Modelling of Moment-Rotation-Settlement Behaviour

When a footing is subjected to cyclic moment loading, due to the repeated rocking of the footing, and the formation of a gap under the unloaded portion of the footing, the soil surface beneath the footing becomes curved (Gajan et al., 2005). By tracking of the shape of the soil surface beneath the footing, the location of the contact area of the footing with soil, and making reasonable assumptions about the shape of the bearing pressure distribution, the moment-rotation-settlement behavior of the foundation is modeled. Applied external loads cause a change in moment magnitude, which causes the changes in contact location and nonlinear bearing pressure distribution. By enforcing equilibrium between the external applied loads and the resisting forces, the moment-rotation relationship and contact geometry are obtained.

Fig. 2 illustrates the contact interface model showing the contact of the rigid footing with the rounded soil surface beneath the footing and the forces acting at the interface. As shown in Fig. 2, soil_min and soil_max represent two different rounded soil surfaces beneath the footing. Soil_max represents the soil surface that contains the maximum settlement experienced by the footing, whereas soil_min represents the surface that exists after the footing leaves the contact with the soil surface as the building rocks. The difference between soil_max and soil_min is conceptually attributed to elastic rebound and bulging of soil into the gap associated with plastic compression in neighboring loaded areas. The footing is modeled with finite number of nodes, each of which corresponds to a node at soil_min surface and soil_max surface.

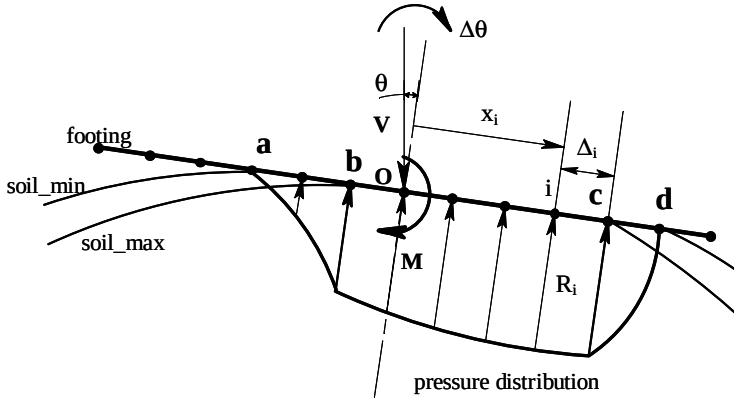

Figure 2. Contact interface model for cyclic moment loading

For every increment in rotation, the contact length of the footing with the soil, contact points with soil surfaces (soil_min and soil_max), and the bearing pressure distribution along the contact length are updated. Every node has the history of following internal variables that are updated for every loading increment: location of footing, current soil surface location (soil_min), maximum past settlement (soil_max), and current bearing pressure. The following procedure explains the method of computation of moment-rotation-settlement relationship in contact interface model when the foundation is subjected to cyclic moment loading. The footing is in contact with the soil_max surface between points b and c and with the soil_min surface between points a and d (Fig. 2).

Procedure of Computation

Step 1

When the incremental rotation $\Delta\theta$ is applied to the footing, the point of rotation, i.e., the point on the footing that neither settles nor uplifts is assumed. In the first iteration, the center of rotation is assumed to be at point b. The new location of the footing is updated at every node:

$$\Delta s\_foot_i = (i - center) \cdot \Delta_i \cdot [\tan(\theta_{incr}) - \tan(\theta_{incr-1})] \quad (1a)$$

$$\Delta\theta = \theta_{incr} - \theta_{incr-1} \quad (1b)$$

where Δs_foot_i is the incremental settlement at footing node i, center is the node number that corresponds to the center of rotation Δ_i is the spacing between nodes (Fig. 2).

Step 2

The shape and the elevation (settlement) of the soil_max surface beneath the footing are updated according to the new position of the footing. This is done by comparing the previous (incr-1) soil_max layer and current footing location. If the footing settles more than the previous soil_max layer at any node, the soil_max layer is updated with the current footing location at that node; otherwise the soil_max layer remains as it is in the previous increment. Once the location of footing and soil_max layer are updated the new end contact nodes of footing and soil_max layer are updated.

Step 3

The new position of the soil_min surface is located using a parameter called the "rebounding ratio" (Rv) and footing position. For the nodes that have the footing and soil in contact during the previous increment and lose contact in current increment the new soil_min surface is updated; the soil_min location for other nodes remain as they are in the previous increment.

$$\Delta soil\_min_{i,incr} = Rv \cdot (soil\_max_{i,incr-1}) \quad (2)$$

The rebounding parameter is related to initial static vertical factor of safety, FS_V, so that a lower FS_V footing would get less rebound and more permanent settlement than a higher FS_V footing.

$$Rv = Rv_0 \cdot \left[1 - \frac{1}{FS_V}\right] \quad (3)$$

Once the location of footing and soil_min layer are updated the new end contact nodes of footing and soil_min profile are updated.

Step 4

The new bearing pressure distribution at every node that has the footing in contact with the soil_max surface (between nodes b and c) is calculated next.

$$R_{i,incr} = R_{i,incr-1} + \frac{Kv \cdot ds}{(V_{ULT}/L)} \quad (4)$$

where, $ds = soil\_max_{i,incr} - soil\_max_{i,incr-1}$

In eq. 4, R_i is a dimensionless bearing pressure parameter that indicates the amount of bearing resistance at node i. The vertical stiffness of the soil per unit length of the footing, Kv (kN/m^2), is normalized by V_{ULT}/L to make R dimensionless. At each node where the footing remains in contact with soil_max profile, the increment of soil_max surface is equal to ds. ds includes the total settlement at that node (both elastic and plastic). The elastic part would be recovered if that node is later unloaded.

Step 5
The pressure distribution at nodes where the footing is in contact with the soil_min layer, but not soil_max layer (i.e., between a and b, and c and d in Fig 2), is modeled by a power law with zero pressures at the extreme contact points (points a and d).

At loading side, between points c and d,

$$R_{i,incr} = \left[\frac{d-i}{d-c}\right]^{n\_load} \cdot R_{c,incr} \tag{5a}$$

and at unloading side, between a and b,

$$R_{i,incr} = \left[\frac{i-a}{b-a}\right]^{n\_unload} \cdot R_{b,incr} \tag{5b}$$

The exponents n_load and n_unload vary gradually when the footing is unloaded so that the change in moment-rotation relationship is gradual. The minimum and maximum values of the exponents n_load and n_unload are 0.5 and 2.0 respectively, in which cases the pressure distributions are parabolic with shapes indicated in Fig. 2.

Step 6
Once the new pressures at all nodes that have footing and soil (soil_min or soil_max) in contact are calculated, the pressures at the other nodes are set to zero, since no tensional resistance is provided by soil. It is important to make sure that, at every node, R_i should satisfy,

$$0.0 \le R_i \le 1.0 \tag{6}$$

If the normalized pressure at any node exceeds 1.0, it is set to be 1.0, as $R_i = 1.0$ indicates that node i experiences the ultimate bearing pressure.

Step 7
The distribution of normalized bearing pressure along the contact length is integrated to get the total resisting vertical force, V_R.

$$V_R = qult \cdot \sum_{i=a}^{d} \left[R_i \cdot \Delta_i \cdot \cos(\theta)\right] \tag{7}$$

where, Δ_i is the distance between nodes i and (i+1). The known applied vertical force, (V = Vapp), is compared with the calculated total vertical resistance force V_R. If vertical equilibrium is satisfied within allowable tolerance, the next step (step 8) follows. If equilibrium is not satisfied, the procedure goes back to step 1 with a new assumed center of rotation. Iteration on steps 1-7 is repeated until vertical equilibrium is achieved.

Step 8
The moment is calculated by integrating the product of bearing force distribution and distance along the contact length of the footing.

$$M = qult \cdot \sum_{i=a}^{d} \left[R_i \cdot \Delta_i \cdot x_i\right] \tag{8}$$

where, x_i is the distance of node i from footing base center point O.

Step 9
The incremental settlement (or uplift) due to rotational loading is obtained from the incremental change in the vertical location of the middle node (O) of the foundation.

This nine-step procedure is used for any increment of cyclic rotation When the loading direction is reversed at any time of loading, the same procedure is followed with loading and unloading sides switched (a and b to c and d and vise versa).

Ultimate Moment and Critical Contact Length Ratio
As the magnitude of rotation is increased, the contact length becomes smaller and moves towards the edge of the footing due to uplift at the other side. As the contact length decreases, the bearing resistance intensity along the contact length increases in order to satisfy vertical equilibrium. As shown in Fig. 3, at one stage, the bearing resistance along the whole contact length becomes equal to the ultimate bearing resistance; hence, no further reduction in contact length is possible. This minimum contact length is defined as the critical contact length (Lc), which can be calculated from bearing capacity equations proposed by Hansen (1970) and Hanna and Meyerhof (1981).

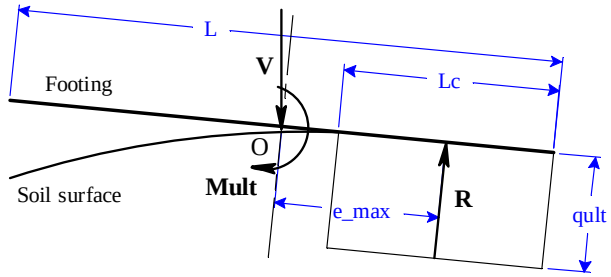

Figure 3. Critical contact length and ultimate moment

For a surface footing, when the contact length is equal to Lc,

$$V = (Lc \cdot B) \cdot \left[\frac{1}{2} \cdot \gamma \cdot B \cdot N_\gamma\right] \cdot \left(1 - 0.4 \cdot \frac{B}{Lc}\right), \text{ when } Lc > B \quad (9b)$$

$$V = (Lc \cdot B) \cdot \left[\frac{1}{2} \cdot \gamma \cdot Lc \cdot N_\gamma\right] \cdot \left(1 - 0.4 \cdot \frac{Lc}{B}\right), \text{ when } Lc < B \quad (9b)$$

Where V is the applied vertical load, B is the width of the footing (B < L), γ is the unit weight of soil, and N_γ is a bearing capacity factor. For a surface footing, neglecting the effect of shape factor, it can be shown that,

$$\frac{Lc}{L} = \frac{1}{FS_V}, \text{ when } FS_V < \frac{L}{B} \quad (10a)$$

$$\frac{Lc}{L} = \left[\frac{1}{FS_V} \cdot \frac{B}{L}\right]^{\frac{1}{2}}, \text{ when } FS_V > \frac{L}{B} \quad (10b)$$

where FS_V is the initial static vertical factor of safety and is given by,

$$FS_V = \frac{V_{ULT}}{V} = \frac{(L \cdot B) \cdot \left[\frac{1}{2} \cdot \gamma \cdot B \cdot N_\gamma\right]}{V} \quad (11)$$

The moment obtained when the contact length reaches the critical contact length, Lc, is defined as the ultimate moment (M_{ULT}), and can be obtained by,

$$M_{ULT} = \frac{V \cdot L}{2} \cdot \left[1 - \frac{Lc}{L}\right] \quad (12)$$

CENTRIFUGE EXPERIMENTS

Several series of experiments have been conducted in a 9.1 m radius centrifuge at the Center of Geotechnical Modeling at the University of California, Davis at 20g centrifuge acceleration. Each series of experiment included models of shear wall structures supported by shallow foundations subjected to lateral cyclic and dynamic loading conditions. The models were tested on a uniform soil bed (Dry Nevada Sand, Dr = 80% and 60%) prepared in a rigid container. All the results in this paper are presented in prototype units unless otherwise stated. Experimental setups, testing procedures and the method of data processing for all lateral cyclic and dynamic tests are explained in detail in Kutter et al. (2005) and Gajan et al. (2004).

The initial static vertical factors of safety (FS_V) of the footings were varied from about 2.0 to 15.0, by changing the weight of the structure, footing geometry and depth of embedment. The applied normalized moment-to-shear ratio ($M/(H \cdot L)$) at the base center point of the footing varied by changing the height at which lateral loading was applied. (Note that H represents the horizontal load, and M/H is the height at which the horizontal load is applied). In this paper, experiments with one particular moment-to-shear ratio are presented ($M/(H \cdot L) = 1.75$) and the effect of FS_V on model simulations are discussed.

Table 1. Model input parameters used for simulations of centrifuge experiment

Test Number	B (m)	L (m)	D/B	V_{ULT} (kN)	FS_V	Kv (MN/m)	$M/(H \cdot L)$
SSG02_05	0.65	2.8	0	1500	2.6	560	1.75
KRR02_04	0.65	2.8	0	1250	3.4	560	1.75
SSG02_03	0.65	2.8	0	1500	5.2	560	1.75
SSG02_04	0.65	2.8	0	1500	7.3	560	1.75
SSG03_03	0.65	2.8	1	3850	14.0	620	1.75

Table 1 presents the properties of the soil and structure used in the selected lateral cyclic experiments that are used in contact interface model simulations presented in this paper. All tests involve a rigid shear wall structure supported by a rectangular footing (0.65 m x 2.8 m) and loaded laterally along longer dimension (L) of the footing. Test SSG03_03 involves an embedded footing (D = B) while all other tests shown in Table 1 includes surface footings. The ultimate vertical load, for pure vertical loading (V_{ULT}), is calculated using conventional bearing capacity equations (Hansen, 1970 and Hanna and Meyerhof, 1981). The static vertical factor of safety FS_V, for pure vertical loading is the ultimate vertical load divided by the weight of the structure used in that particular experiment. Gazetas solutions for rigid footing (Gazetas, 1991) are used to calculate initial vertical stiffness of the foundation, which is a function of shear modulus (G), Poisson's ratio (ν) and the geometry of the footing. The applied normalized moment to shear ratio ($M/(H \cdot L)$), corresponds to the normalized height of lateral push (h/L, where h is the height of lateral loading from the base of the footing), used in the experiments are shown in the last column of Table 1. All the tests shown in Table 1 were carried out with constant vertical load and approximately constant height of push and therefore FS_V and $M/(H \cdot L)$ ratio remain constant throughout the experiment.

The parameters that are input to the contact interface model include: Length of the footing, ultimate vertical load, initial static vertical factor of safety, and initial vertical stiffness of the foundation. Note

that the rebounding ratio coefficient, Rv_o (eq. 3), is taken as 0.1 for all the simulations, and the parameters that control the shape of the parabolas in bearing pressure, n_load and n_unload (eq. 5a and 5b) are taken as 0.5 and 2.0 respectively. These default values for n_unload, n_load and Rv_o were determined by trial and error to match the entire series of centrifuge experiments as well (Gajan, 2006). The qualitative results of the simulations are not highly sensitive to these assumed values.

COMPARISON OF SIMULATIONS WITH EXPERIMENTS

Based on the experimental measurements, the forces and displacements at the base center point of the footing were calculated using rigid body translation and rotation relations (Gajan, 2006). The experimentally measured rotation time history was given to the contact interface model as an input along with the parameters shown in Table 1 for each test, and the calculated moment and settlement were obtained from contact interface model. Fig. 4 and 5 show the comparisons of contact interface model simulations with the centrifuge experimental results for different FS_V. The moment-rotation and settlement-rotation results presented in Fig. 4 and 5 are referenced to the base center point of the footing during lateral cyclic loading. Fig. 4(a) presents the comparisons for a footing with FS_V = 2.6 (SSG02_05). Simulations for moment-rotation and settlement-rotation relationships compare reasonably well with the observed behavior in the experiment. The moment capacity and the degradation of rotational stiffness with increasing amplitude of rotation are captured well in the model. Though the simulated overall permanent settlement was little less (about 10%) than the experimentally measured settlement, the amounts of permanent settlement per cycle of loading for different amplitude of rotations are within reasonable agreement in both simulations and experiments. Because the factor of safety is relatively small, both the simulation and the experiment show accumulation of permanent settlement for each cycle without significant uplift of the footing.

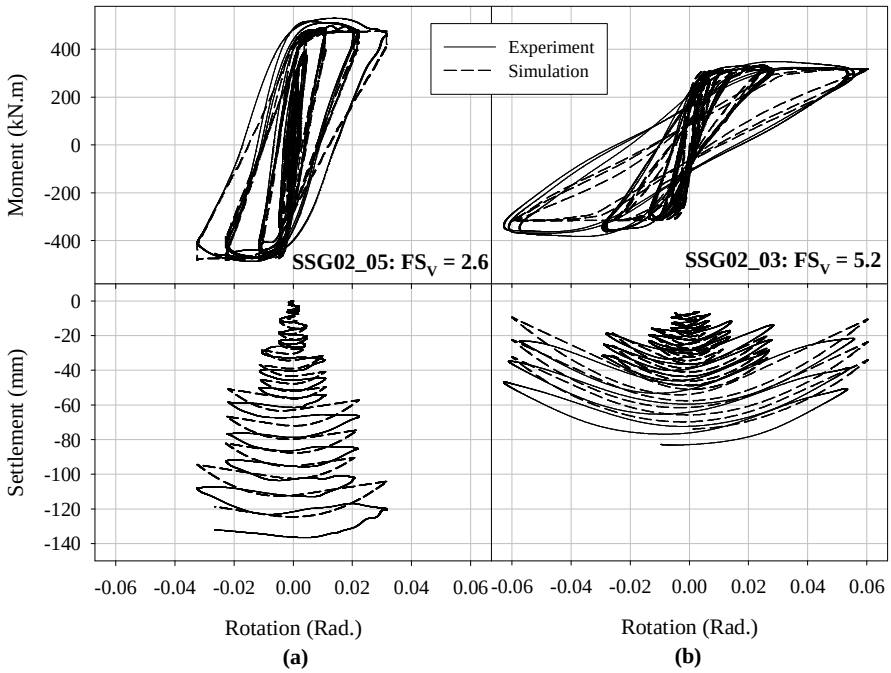

Figure 4. Comparison of contact interface model simulations with experimental results: Moment-rotation and settlement-rotation relationships at the base center point of the footing for lateral cyclic tests with different FS_V

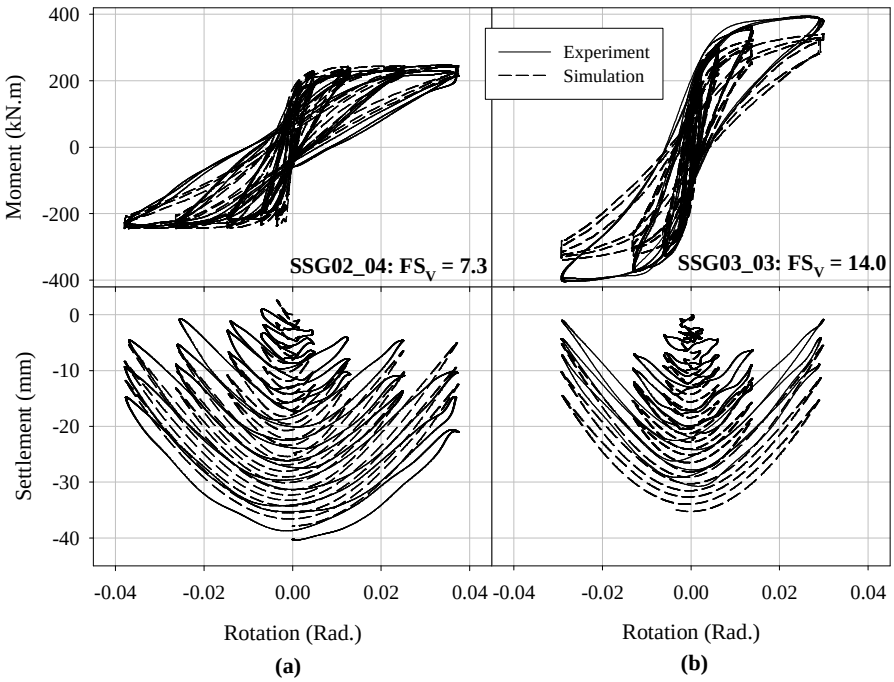

Figure 5. Comparison of contact interface model simulations with experimental results: Moment-rotation and settlement-rotation relationships at the base center point of the footing for lateral cyclic tests with different FS_V

Fig. 4(b) compares the contact interface model simulations with experiments for FS_V = 5.2. The moment-rotation hysteresis loops compare reasonably with the experiments, except for the largest rotation cycles (0.06 Radians), where the simulation shows thin hysteresis loops with less area enclosed by them than the experimental results. The shapes of the settlement-rotation curves are similar in both simulations and experiments with both showing significant uplift during larger rotations. Fig. 5(a) shows the results for FS_V = 7.3. The comparison of simulation with experimental results shows a similar trend observed in the previous two comparisons. In Fig. 5(a), the simulation shows more settlement per cycle than the experiment during the small amplitude cycles, and less settlement per cycle than the experiment during the large amplitude cycles.

Fig. 5(b) shows the simulation and experimental results for the lateral cyclic test SSG03_03, which was an embedded test (D = B) with FS_V = 14.0. The moment capacity observed in the simulation is smaller than the capacity observed in the experiment. Since the test was embedded, it shows larger moment capacity than one would expect for a surface footing. In the simulations, the effect of depth of embedment was included in FS_V through an increase in vertical bearing capacity, but passive resistance of the soil was not included in ultimate lateral load and ultimate moment. Overall, the permanent settlement obtained in the simulation is within 20% of the measured settlement in the experiment.

Ultimate Moment

Fig. 6 shows the ultimate moment obtained in contact interface model simulations and centrifuge experiments for different FS_V foundations. Also included in Fig. 6 are the analytical envelope obtained from eq. 12 (for H = 0) and the bounding surface proposed by Cremer et al., 2001 (for $M/(H \cdot L) = 1.75$) in normalized moment–normalized vertical load space. The contact interface model reproduces the ultimate moment capacities given by eq. 12, which also agree well with the experimental results. Also note that all the experiments and simulations are for $M/(H \cdot L) = 1.75$. It can be seen that the effect of shear on moment capacity is negligible for the moment-to-shear ratio used in the simulations.

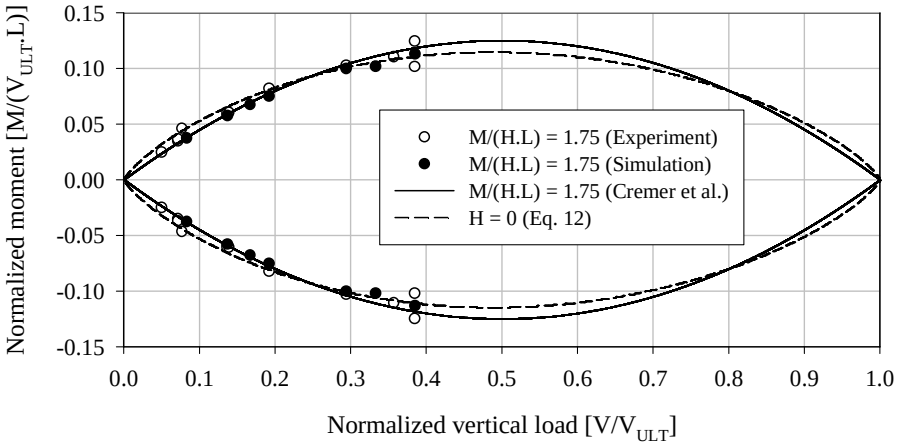

Figure 6. Experimental and model simulation ultimate moment points with analytical bounding surfaces in normalized moment-vertical load plane

Energy Dissipation

Moment-rotation relationships plotted in Figures 4, and 5 clearly indicate that considerable amount of energy is dissipated beneath foundation due to rocking motion. The magnitude of energy dissipation depends on the maximum moment reached in that particular cycle (M_max_cycle), the corresponding cyclic rotation (θ_max_cyc), and the shape of unloading-reloading paths in moment-rotation plane. In an attempt to normalize the amount of energy dissipation, damping ratios (ξ) are calculated according to the following definition (Kramer, 1996).

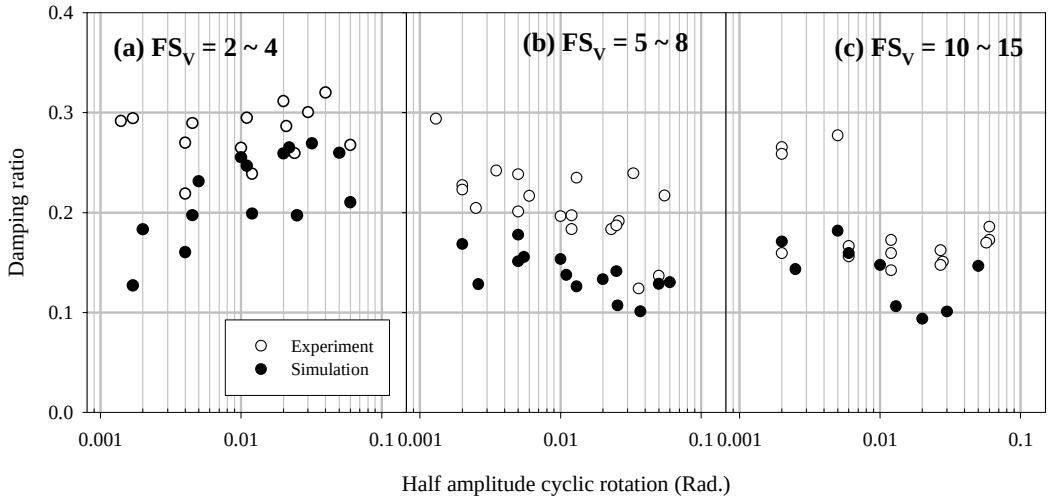

Figure 7: Comparison of model simulation with experimental results: Effect of FS_V on energy dissipation through moment-rotation hysteretic loops

$$\xi = \frac{1}{4 \cdot \pi} \cdot \frac{\text{Area\_of\_M\_}\theta\text{\_hysteresis\_loop}}{\frac{1}{2} \cdot (\text{M\_max\_cyc}) \cdot (\theta\text{\_max\_cyc})} \tag{12}$$

Fig. 7 plots the damping ratio (ξ) observed in centrifuge experiments and simulations per cycle of loading against half amplitude of cyclic rotation for different range of FS_V, but for the same M/(H·L) ratio (1.75). Both experiments and simulations show that as FS_V increases, damping ratio decreases, though, in general, model predictions for damping ratio are smaller than the experimental results.

Though there is scatter in data, the experimentally observed damping ratios and model predictaions fall in the same range for the same FS_V footings.

Permanent Settlement

Fig. 8 compares the model simulation results for normalized permanent settlement per cycle against half amplitude cyclic rotation with experimental results for $M/(H \cdot L) \approx 1.75$ and various FS_V ranges. All these experiments and simulations involve a rectangular footing (L = 2.8 m in the direction of lateral loading), as shown in Table 1. Settlements simulated by the contact interface model follow the same trend followed by the experimental results for the range of FS_V footings tested and for the range of rotations applied.

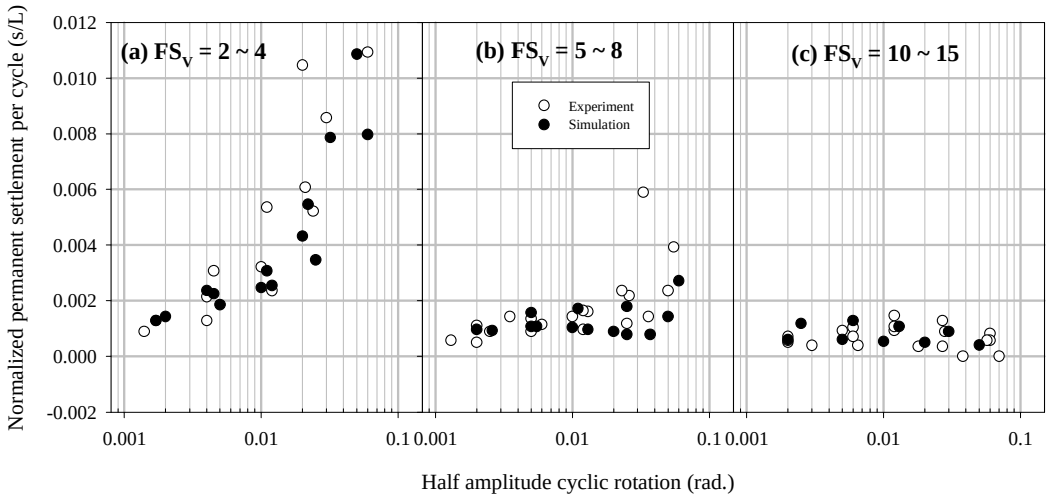

Figure 8. Comparison of model simulations with experimental results: Effect of FS_V on the amount of normalized permanent settlement accumulated beneath the footing

CONCLUSIONS

The contact interface model presented in this paper is shown to be capable of simulating the moment-rotation and settlement-rotation behavior of rocking shallow foundations by tracking the moving contact between a rigid footing and the rounded soil surface beneath the footing. The model is simple, and only five major model parameters need to be input by the user: length of the footing, ultimate vertical load, initial static vertical factor of safety, initial vertical stiffness, and the rebounding ratio of soil. The model captures the essential features of moment-rotation-settlement relationships observed in the centrifuge experiments. The contact interface model predictions for moment capacity, rotational stiffness, energy dissipation through foundation rocking, and accumulated permanent deformations beneath the foundation compare reasonably well with the centrifuge experimental results.

Other researchers have used macro-element modeling concepts to describe the load-deformation behavior of structural elements and shallow foundations. Most of the previous attempts with macro-element models for shallow foundations describe the constitutive relations based on yield surfaces, potential surfaces, and flow rules described in generalized load space. The contact interface model differs in the sense that the constitutive relations are obtained by tracking the evolution of the maximum shape of the gaps, and the geometry of the contact interface. The critical contact length ratio, introduced in this paper, is a key parameter that defines the kinematics of the moving contact.

Extensions of the model to enable simulation of shear-sliding relationships, coupling between moment, shear, and vertical loads, and the coupling between the sliding and rotational modes as well

as additional details associated with the robustness in dynamic finite element simulations (in OpenSEES finite element framework) are described in Gajan (2006).

AKNOWLEDGEMENTS

This research work was supported by the Pacific Earthquake Engineering Research (PEER) Centers Program of the National Science Foundation (NSF) under award number EEC-9701568 and PEER project number 2262001. Any opinions, findings and conclusions or recommendations expressed in this paper are those of the authors and do not necessarily reflect those of the NSF. The authors would like to acknowledge the suggestions and support provided by Geoff Martin, Tara Hutchinson, Ross Boulanger, Boris Jeremic, Dan Wilson, Key Rosebrook, Justin Phalen, and Jeremy Thomas.

REFERENCES

Cremer, C., Pecker, A. and Davenne, L. (2001). "Cyclic macro-element of soil structure interaction: Material and geometrical nonlinearities." *Int. Journal of Num. Anal. Meth. Geomech.*, Vol. 25, 1257-1284.

Faccioli, E., Paolucci, R. and Vivero, G. (2001). "Investigation of seismic soil-footing interaction by large scale cyclic tests and analytical models." *Proc. 4th Int. Conf. Recent Advances in Geotechnical Earthquake Engineering and Soil Dynamics*, San Diego, Calif., March 26-31, 2001

Gajan, S. (2006) "Physical and numerical modeling of nonlinear cyclic load-deformation behavior of shallow foundations supporting rocking shear walls", Ph.D. Dissertation, College of Engineering, University of California, Davis, Calif., 2006

Gajan, S., Kutter, B. L. and Thomas, J. (2005) "Physical and numerical modeling of cyclic moment-rotation behavior of shallow foundations" *Proc. 16th Intl. Conf. Soil Mechanics and Geotechnical Engineering*, Sept., 2005, Osaka, Japan, Vol. 2, 795-798.

Gajan. S., Phalen, J. D., Kutter, B. L., Hutchinson, T. C. and Martin, G. (2004). "Centrifuge modeling of nonlinear cyclic load-deformation behavior of shallow foundations" *Proc. 11th Intl. Conf. Soil Dynamics and Earthquake Engineering and 3rd Intl. Conf. Earthquake Geotechnical Engineering.*, University of California, Berkeley. Calif., Jan. 2004. Vol. 2, pp 742-749

Gajan, S., Phalen, J. D., Kutter, B. L., Hutchinson, T. C. and Martin, G. (2005). "Centrifuge modeling of load-deformation behavior of rocking shallow foundations", *Journal of Soil Dynamics and Earthquake Engineering*, Vol. 25 (7-10), 773-783.

Gazetas, G. (1991). "Foundations Vibrations." Foundation Engineering Handbook, Ch 15, Fang, H. Y. (ed.), Van Nostrand Reinhold, New York.

Hanna, A. M. and Meyerhof, G. G. (1981). "Experimental Evaluation of Bearing Capacity of Footings Subjected to Inclined Loads," *Canadian Geotechnical Journal*, Vol. 18, No. 4, 559-603.

Hansen, J. B. (1970). "A Revised and Extended Formula for Bearing Capacity," Danish Geotechnical Institute, Bulletin 28, Copenhagen

Houlsby, G. T., Cassidy, M. J. (2002). "A plasticity model for the behavior of footings on sand under combined loading." *Geotechnique*, Vol. 52, No. 2, 117 – 129.

Kutter, B. L., Martin, G., Hutchinson, T. C., Harden, C., Gajan. S. and Phalen, J. D. (2006). "Workshop on modeling of nonlinear cyclic load-deformation behavior of shallow foundations." PEER Workshop, University of California, Davis, PEER Report No. 2005/14.

Nova, R. and Montrasio, L. (1991). "Settlements of shallow foundations on sand." *Geotechnique*, Vol. 41, No. 2, 243 – 256.

Taylor, P. W., Bartlett, P. E. and Weissing, P. R. (1981). "Foundation Rocking under Earthquake Loading," *Proc. of the 10th Intl. Conf. on Soil Mechanics and Foundation Engineering*, Vol. 3, 33-322.